Temporal and Acoustic Accuracy of an Implicit Upwind Method for Ducted Flows

Jeffrey P. Ridder* and Robert A. Beddini†
University of Illinois at Urbana-Champaign, Urbana, Illinois 61801

An implicit, time-accurate method for ducted-flow aeroacoustics is presented. The method is unfactored, using line Gauss-Seidel relaxation and multiple axial sweeps for convergence of each time step. First- or higher-order upwind spatial differencing is accomplished using either a modified form of van Leer's flux vector splitting or Roe's flux difference splitting on the inviscid terms of the governing equations. A general time integration algorithm is employed, which encompasses several schemes including the Euler implicit method used for the current work. Results are presented from three numerical tests with comparisons being made to both theory and experiment. These spatial and temporal accuracy tests show excellent tracking of the acoustic wave speed using Roe's flux difference splitting. The method is further seen to reflect waves properly as demonstrated by comparison of computed pressure amplitudes and acoustic mode shapes with experimental data. Additionally, no low mean-flow Mach number convergence limitation is observed. No Courant number stability restriction is displayed, as accurate results are obtained utilizing Courant numbers of order 10^2 for these tests.

Nomenclature

a = speed of sound
E = total specific energy
F = x inviscid flux vector
F_v = x viscous flux vector
G = y inviscid flux vector
G_v = y viscous flux vector
H = z inviscid flux vector
H_v = z viscous flux vector
I = identity matrix
L = longitudinal chamber length
M = Mach number
N = flux tensor
n = unit outward normal to surface
p = pressure
Q = vector of dependent variables
q = heat flux vector
T = right eigenvector matrix
t = time
u = velocity vector
u = x velocity component
v = y velocity component
w = z velocity component
x = axial coordinate
y = transverse coordinate (depth)
z = transverse coordinate (height)
β = time integration parameter
Δ = increment in space
δ = increment in time
κ_x = differencing parameter
Λ = diagonal eigenvalue matrix
λ = piston displacement
θ = time integration parameter
ρ = density
ρ' = density amplitude about the mean
τ = viscous stress tensor

Subscripts

i = x index
j = y index
k = z index
L = left interface state
R = right interface state
s = surface condition
v = viscous flux vector

Superscripts

n = time level
$+$ = forward moving characteristic
$-$ = backward moving characteristic
$\sim$ = quantity evaluated using Roe-averaged variables

I. Introduction

THOUGH significant progress has been made in developing and applying multidimensional computational methods to steady-state aerodynamics and propulsion problems, satisfactory time-accurate methods for compressible flows are a present research issue. The partial enclosure provided by propulsion chambers often favors the development of oscillatory flows. Small amplitude (acoustic) modes or nonlinear disturbances can interact with propellant combustion processes to produce instability. There are a variety of physical mechanisms that may cause instability in any given system (see, for example, Williams[1] or Strehlow[2]) and these must be assessed on an individual basis. Generally, however, the time and space scales of combustion, turbulence, acoustic modes, and mean flow may differ by orders of magnitude. The computational investigation of instability mechanisms (or other transient behavior) therefore requires robust, efficient, and accurate algorithms.

Demonstration of acoustic mode and traveling shock wave predictive capability in relatively simple ducted compressible flow environments is the second step in assessing the accuracy of computational methods (the first is usually an assessment of spatial accuracy in steady-state flows). Several recent computational methods used in such studies may be classified into two groups:

Presented as Paper 89-2554 at the AIAA/ASME/ASEE/SAE 25th Joint Propulsion Conference, Monterey, CA, July 10–13, 1989; received Dec. 21, 1989; revision received July 31, 1990; accepted for publication Aug. 13, 1990.

*Graduate Student, Department of Aeronautical and Astronautical Engineering. Student Member AIAA.

†Associate Professor, Department of Aeronautical and Astronautical Engineering. Associate Fellow AIAA.

1) Explicit methods, such as those used by Kailasanath et al.,[3] Yang et al.,[4] and Vuillot and Avalon,[5] have been implemented with first-order upwind differencing (and thus retain propagation accuracy along characteristics), and are highly vectorizable. However, they are subject to time step stability constraints (CFL numbers of order unity), which can limit resolution of small spatial features or lead to significant CPU times in their resolution.

2) Approximately factored implicit methods are frequently implemented with alternating direction implicit (ADI) spatial factorization (Lindemuth and Killeen,[6] Beam and Warming,[7] Briley and McDonald[8]). They have been applied to unsteady flow problems by Baum and Levine[9] and Tang et al.[10] Approximately factored methods have a demonstrated advantage at resolving multispatial scale features (such as thin acoustic boundary layers along duct surfaces[9]). They are usually implemented as central difference methods with artificial damping to achieve second-order spatial accuracy. Most critically, they are limited to CFL numbers of order unity due to first-order time splitting truncation error.[11]

Recent interest in characteristic-based schemes has been stimulated to a great degree by a need for improved shock capturing in high-speed flowfields. Two major classes of upwind methods have resulted. The first is the flux vector splitting (FVS) method such as those developed by Steger and Warming[12] or van Leer.[13] The second is the flux difference splitting (FDS) scheme introduced by Roe.[14] Since these schemes preserve the characteristic behavior of the governing equations, they offer the possibility of time-accurate resolution of unsteady acoustic waves. The steady-state spatial resolution of van Leer's method and Roe's method has been compared by van Leer et al.,[15] with Roe's FDS method proving superior.

These methods have also stimulated interest in unfactored algorithms. Chakravarthy[11] and Thomas and Walters[16] have been among the proponents of iterative upwind methods. Each has cited the possibility of achieving steady-state solutions as rapidly as factored schemes, while offering the flexibility of time-accurate solutions as well. A fully iterative algorithm (with no factored directions) avoids factorization error and, therefore, permits larger CFL numbers.

The objective of this work is to develop an implicit time-accurate method capable of capturing propulsion chamber acoustics. The axisymmetric and three-dimensional Navier-Stokes equations are used for the cases of interest. The algorithm is iterative, using line Gauss-Seidel relaxation. The boundary conditions are implicit and characteristic-based for proper reflection of waves. The unsteady behavior of the two upwind schemes mentioned is demonstrated by use of three separate numerical experiments to test for acoustic accuracy.

II. Numerical Method

Governing Equations

Although both the axisymmetric and three-dimensional Navier-Stokes equations are employed in this work, only the three-dimensional method is described here since the axisymmetric algorithm is similar. The three-dimensional Navier-Stokes equations may be represented in integral form as

$$\frac{\partial}{\partial t}\int\int\int_V \boldsymbol{Q}\,dV + \int\int_S \boldsymbol{N}\cdot\boldsymbol{n}\,dS = 0 \tag{1}$$

$\boldsymbol{Q}$ is the vector of conserved variables, $\boldsymbol{Q} = [\rho, \rho u, \rho v, \rho w, \rho E]^T$. The flux tensor $\boldsymbol{N}$ is given in strong conservation law form as

$$\boldsymbol{N} = (F - F_v)\boldsymbol{i} + (G - G_v)\boldsymbol{j} + (H - H_v)\boldsymbol{k} \tag{2}$$

and,

$$\boldsymbol{n} = n_x\boldsymbol{i} + n_y\boldsymbol{j} + n_z\boldsymbol{k} \tag{3}$$

$$F - F_v = \begin{bmatrix} \rho u \\ \rho u^2 + p - \tau_{xx} \\ \rho uv - \tau_{xy} \\ \rho uw - \tau_{xz} \\ (\rho E + p)u + q_x - u\tau_{xx} - v\tau_{xy} - w\tau_{xz} \end{bmatrix} \tag{4a}$$

$$G - G_v = \begin{bmatrix} \rho v \\ \rho uv - \tau_{xy} \\ \rho v^2 + p - \tau_{yy} \\ \rho vw - \tau_{yz} \\ (\rho E + p)v + q_y - u\tau_{xy} - v\tau_{yy} - w\tau_{yz} \end{bmatrix} \tag{4b}$$

$$H - H_v = \begin{bmatrix} \rho w \\ \rho uw - \tau_{xz} \\ \rho vw - \tau_{yz} \\ \rho w^2 + p - \tau_{zz} \\ (\rho E + p)w + q_z - u\tau_{xz} - v\tau_{yz} - w\tau_{zz} \end{bmatrix} \tag{4c}$$

The system is closed by assuming a calorically perfect gas and Fourier's law for the heat flux vector $\boldsymbol{q}$.

Currently, a uniformly spaced Cartesian grid is used for simplicity. Integrating Eq. (1) over a grid cell in the computational domain with center at i, j, k gives

$$\left(\frac{\partial \boldsymbol{Q}}{\partial t}\right)_{i,j,k} + \frac{1}{\Delta x}[(F - F_v)_{i+\frac{1}{2}} - (F - F_v)_{i-\frac{1}{2}}] + \frac{1}{\Delta y}[(G - G_v)_{j+\frac{1}{2}} - (G - G_v)_{j-\frac{1}{2}}] + \frac{1}{\Delta z}[(H - H_v)_{k+\frac{1}{2}} - (H - H_v)_{k-\frac{1}{2}}] = 0 \tag{5}$$

where Q is now an average value for the entire grid cell centered at i, j, k.

The two-dimensional equation system for an axisymmetric flow follows the form suggested by Peyret and Viviand,[17] and includes additional source terms that reduce the governing equations to a weakly conservative form.

Time Integration

Time integration for this work is first order using the Euler implicit method. Extensions to higher order may be made by using the general time integration formula given by Warming and Beam,[18]

$$\left\{\frac{1}{\delta t}I + \frac{\theta}{1+\beta}\left[\frac{\partial}{\partial x}\frac{\partial(F - F_v)}{\partial \boldsymbol{Q}} + \frac{\partial}{\partial y}\frac{\partial(G - G_v)}{\partial \boldsymbol{Q}} + \frac{\partial}{\partial z}\frac{\partial(H - H_v)}{\partial \boldsymbol{Q}}\right]^n\right\}\delta \boldsymbol{Q}^n = -\frac{1}{1+\beta}\left[\frac{\partial}{\partial x}(F - F_v) + \frac{\partial}{\partial y}(G - G_v) + \frac{\partial}{\partial z}(H - H_v)\right]^n + \frac{\beta}{(1+\beta)}\frac{\delta \boldsymbol{Q}^{n-1}}{\delta t} + O\left[\left(\theta - \beta - \frac{1}{2}\right)\delta t + \delta t^2\right] \tag{6}$$

where

$$\delta \boldsymbol{Q}^n = \boldsymbol{Q}^{n+1} - \boldsymbol{Q}^n \tag{7}$$

Some of the integration schemes associated with Eq. (6) are given in Table 1.

Table 1 Time integration schemes of Eq. (6)

θ	β	Scheme	Truncation error
0	0	Euler, explicit	$O(\delta t)$
0	$-\frac{1}{2}$	Leapfrog, explicit	$O(\delta t^2)$
$\frac{1}{2}$	0	Crank-Nicolson, implicit	$O(\delta t^2)$
1	0	Euler, implicit	$O(\delta t)$
1	$\frac{1}{2}$	3-point backward, implicit	$O(\delta t^2)$

Table 2 Differencing schemes for Eq. (16)

κ_x	Differencing scheme
-1	Fully upwind
$+1$	Central difference
$\frac{1}{3}$	Third-order upwind biased
0	Fromm's scheme

Spatial Differencing

The diffusive (viscous and heat flux) terms of the governing equations are treated implicitly using second-order central differences. The inviscid (convective and pressure gradient) terms are solved using one of the upwind methods introduced previously. These are outlined briefly in the following section.

Modified van Leer Flux Vector Splitting

Flux vector splitting methods split the convective flux vectors into nonpositive and nonnegative components via the eigenvalues of the convective flux Jacobian matrix. For example, flux vector $\boldsymbol{F}$ is split as follows:

$$A(\boldsymbol{Q}) = \frac{\partial \boldsymbol{F}}{\partial \boldsymbol{Q}} = T\Lambda T^{-1} \tag{8}$$

where the columns of T are the eigenvectors of A. The symbol Λ is the diagonal eigenvalue matrix

$$\Lambda = \begin{bmatrix} \lambda_1 & & 0 \\ & \ddots & \\ 0 & & \lambda_5 \end{bmatrix} \tag{9}$$

that may be split into positive and negative (or forward and backward moving) components,

$$\Lambda = \Lambda^+ + \Lambda^- \tag{10}$$

Likewise,

$$A = A^+ + A^- \tag{11}$$

and, due to homogeneity,

$$\boldsymbol{F} = (A^+ + A^-)\boldsymbol{Q} = \boldsymbol{F}^+ + \boldsymbol{F}^- \tag{12}$$

van Leer's flux vector splitting[13] is chosen over other flux vector splitting methods because of its smooth transition across sonic points. The modification of Hanel et al.[19] has been applied due to improved energy conservation in regions of strong Mach number gradients over the original van Leer splitting. If $M_x = u/a$, then for $|M_x| < 1$ and with $\boldsymbol{F}^{\pm}_{\text{mass}} = \pm\rho(a/4)(M_x \pm 1)^2$,

$$\boldsymbol{F}^{\pm} = \begin{bmatrix} \boldsymbol{F}^{\pm}_{\text{mass}} \\ \boldsymbol{F}^{\pm}_{\text{mass}}[(\gamma-1)u \pm 2a]/\gamma \\ \boldsymbol{F}^{\pm}_{\text{mass}} v \\ \boldsymbol{F}^{\pm}_{\text{mass}} w \\ \boldsymbol{F}^{\pm}_{\text{mass}}[E + (p/\rho)] \end{bmatrix} \tag{13}$$

When $|M_x| \geq 1$,

$$\begin{aligned} \boldsymbol{F}^+ &= \boldsymbol{F}, & \boldsymbol{F}^- &= 0 & M_x &\geq +1 \\ \boldsymbol{F}^+ &= 0, & \boldsymbol{F}^- &= \boldsymbol{F} & M_x &\leq -1 \end{aligned} \tag{14}$$

The remaining inviscid flux vectors follow similarly.

The split flux vectors are upwinded individually using the MUSCL differencing technique.[20] With MUSCL,

$$\boldsymbol{F} = \boldsymbol{F}^+(\boldsymbol{Q}^-) + \boldsymbol{F}^-(\boldsymbol{Q}^+) \tag{15}$$

where,

$$\boldsymbol{Q}^{\mp}_{i\pm\frac{1}{2}} = \boldsymbol{Q}_i \pm \frac{\phi}{4}[(1 \mp \kappa_x)\nabla_x + (1 \pm \kappa_x)\Delta_x]\boldsymbol{Q}_i \tag{16}$$

First-order upwind differencing is selected when $\phi = 0$. Otherwise, higher-order schemes may be chosen when $\phi = 1$ by selecting the appropriate value of the parameter κ_x from Table 2.

Roe's Flux Difference Splitting

Godunov[21] proposed a method for the solution of hyperbolic systems of equations whereby the flux across the cell interface is solved exactly to simulate the motion of shocks and expansion fans. Due to the expense of Godunov's method, the concept of flux difference splitting was introduced by Roe[14] as an approximate solution to the Riemann problem to obtain the fluxes at a cell interface. The flux vector, $\boldsymbol{F}$, may be determined at the $i + \frac{1}{2}$ interface as

$$\boldsymbol{F}_{i+\frac{1}{2}} = \tfrac{1}{2}[\boldsymbol{F}_L + \boldsymbol{F}_R - |\tilde{A}|(\boldsymbol{Q}_R - \boldsymbol{Q}_L)] \tag{17}$$

where the subscripts L and R represent states to the left and to the right of the interface, respectively. The values of $\boldsymbol{Q}$ at these locations are given by the MUSCL differencing scheme of Eq. (16), where L corresponds to $-$ and R corresponds to $+$. The $\sim$ overscript designates a quantity evaluated using Roe-averaged variables. These variables are given by Roe in Ref. 14. The flux difference Jacobian is given as

$$|\tilde{A}| = \tilde{A}^+ - \tilde{A}^- \tag{18}$$

where,

$$\tilde{A}^{\pm} = \tfrac{1}{2}\tilde{T}(\tilde{\Lambda} \pm |\tilde{\Lambda}|)\tilde{T}^{-1} \tag{19}$$

The flux vector may then be approximately linearized as follows:

$$\begin{aligned} \boldsymbol{F}^{n+1}_{i+\frac{1}{2}} = \boldsymbol{F}^n_{i+\frac{1}{2}} &+ \tfrac{1}{2}[A^n_L + |\tilde{A}|^n_{i+\frac{1}{2}}]\delta\boldsymbol{Q}^n_L \\ &+ \tfrac{1}{2}[A^n_R - |\tilde{A}|^n_{i+\frac{1}{2}}]\delta\boldsymbol{Q}^n_R \end{aligned} \tag{20}$$

Iteration Method

Application of higher-order upwind differencing operators to the inviscid terms of the three-dimensional governing equations results in a 13-block diagonal matrix structure. The time splitting error introduced by factored schemes results in a CFL number limitation that restricts the possible benefit of implicit methods for unsteady flows. It is for this reason that an iterative scheme has been implemented in this work.

Line Gauss-Seidel relaxation is used with successive backward and forward sweeping in the axial direction. After each axial sweep, the transverse and axial sweep directions are alternated (from backward to forward or vice versa). The transverse sweep is alternated to its orthogonal counterpart after every second axial sweep (i.e., from j to k or vice versa) so as to prevent any possible bias in the crossplanes. The remaining line is solved as a block pentadiagonal for higher-

order crossplanes or a block tridiagonal for first-order crossplanes. Time-accurate solutions typically require a minimum number of axial sweeps for convergence to within a specified tolerance. For the calculations presented here, six sweeps were found to be sufficient for convergence of the normalized change of the dependent variables (determined globally) to within 0.1%.

The differencing scheme chosen is restricted by the sufficient (not necessary) condition of diagonal dominance for convergence of an iterative method. Diagonal dominance is lost when higher-order spatial differencing operators are used. Convergence is then found to depend on the particular splitting method used as well as flow conditions and computational parameters (e.g., Courant number). For the problems discussed here, the second-order van Leer scheme is found to converge while second-order Roe generally does not. For the third test case to be discussed, a hybrid operator (second-order Roe axially and first-order Roe radially) is found to be convergent. The advantage of this mixed operator becomes obvious when the effect of the large aspect ratio of the cells (approximately 200:1) on truncation error is considered.

Boundary Conditions

Due to the higher-order upwind differencing, information is required at two additional phantom cells outside the computational domain. The boundary conditions are characteristic based with the number of conditions specified being equal to the number of characteristics pointing into the computational domain from the boundary. The remaining computationally required conditions are then extrapolated from the computational domain to the boundary (corresponding to characteristics pointing outward from the computational domain to the boundary).

The conditions specified at the boundary interface (e.g., pressure at a subsonic exit) serve as the point of expansion for a one-sided extrapolation to the exterior phantom cells. To complete the computationally required information, a simple (one-sided) extrapolation to the exterior domain is performed by truncating the expansion of the remaining variables at a higher-order derivative (e.g., $\partial^2 T/\partial x^2 = 0$, $\partial^2 u/\partial x^2 = 0$, etc., for a subsonic exit condition). The phantom cells, then, are expressed in terms of the two nearest interior cells and the specified information at the boundary.

In the test calculations to follow, a resonance tube (enclosed duct with a harmonically moving piston at the duct end, $x = L$) is considered. The piston boundary condition used for this case is described as follows. Formal solution on a grid fixed in computational space would require a time-varying coordinate mapping to accommodate piston displacement, $\lambda(t)$. However, since $\lambda/L \ll 1$ in the experiment, the computational geometry is assumed fixed and the flow velocity is equated to the piston velocity at that boundary. The pressure gradient is not assumed negligible and is specified by considering a one-dimensional Euler equation at the interface,

$$\frac{\partial p}{\partial x} = -\rho \frac{\partial u}{\partial t} - \rho u \frac{\partial u}{\partial x} \tag{21}$$

where u and $\partial u/\partial t$ are specified analytically by the harmonic piston displacement function, $\lambda(t)$, at the piston boundary. The axial velocity gradient, $\partial u/\partial x$, is determined by a second-order extrapolation to the boundary. This higher-order expression for pressure minimizes the excitation of false harmonics.

A consequence of assuming a fixed computational boundary for a harmonically varying piston motion is the addition or depletion of mass into the computational domain. The amount of mass added may be determined by considering the equation for conservation of mass over a cycle for the posed problem:

$$m = -A \int_{\text{cycle}} \rho(t,L)\dot{\lambda}\,dt \tag{22}$$

where $A(L)$ is the cross-sectional area of the duct at the boundary and flow properties have been assumed to be approximately one-dimensional there. Since $\rho(t,L)$ and $\dot{\lambda}$ can be out of phase by more than 90 deg (depending on acoustic amplitude, computational method, and computational conditions), system mass need not be conserved, and was observed to increase in preliminary acoustic calculations. As an example, for an acoustic density response 180 deg out of phase with velocity at the piston boundary, the global increase in density may be found to be

$$\Delta\rho = \frac{\rho' \lambda_{\max} \pi}{L} \tag{23}$$

where ρ' is the amplitude of the density about the mean and $\lambda_{\max}$ is the amplitude of the piston displacement. Similarly, it may be shown that the global density increase is zero when the density response is a shock.

To compensate for the change in system density requires that each cell be treated individually since the exact density amplitude and mode shape at each location varies and is not known a priori. This is accomplished by determining the mean density at each grid cell over a cycle. This is then compared to the theoretical ambient mean, and the difference is removed from the current value of density at the end of the cycle. This procedure was found to conserve mass properly in the calculations presented here. Global conservation corrections for momentum and energy were not taken into account, since these are of higher-order for low amplitude acoustics, and their change over several cycles was not as apparent as the system mass change prior to applying the corrective procedure.

III. Results and Discussion

The time-accurate behavior of this algorithm for chamber flows has been examined by testing for acoustic accuracy. Acoustic accuracy in a numerical method may be evaluated in terms of two critical guidelines. The first is the ability of the method to track a small disturbance to be traveling at its proper acoustic wave speed. The second is the ability of the numerical boundary conditions to reflect the disturbance without any losses or gains, thereby preserving acoustic modal accuracy. Three test cases have been considered to examine the spatial and temporal accuracy of the method by comparison to experiment and theory. All results presented here are first-order accurate in time using the Euler implicit method. The Crank-Nicolson method ($\theta = \frac{1}{2}$) was also tried and presented some difficulty. In particular, in the resonance tube test case it was found that severe overshoots of the traveling shocks occurred and caused instability. It is expected that an appropriate flux limiter applied to the implicit side of the integration procedure would alleviate this problem.

ONERA Cold Flow Test

The spatial accuracy of the method is first examined by comparison to experimental data from an ONERA cold flow experiment.[22] The chamber is shown in Fig. 1. The computational geometry was nozzleless with a $28 \times 10 \times 10$ grid and quarter cross-plane symmetry. The upper and lower surfaces were injected with $(\rho w)_s = 13.02$ kg/m^2/s. The wall boundary conditions were adiabatic and resulted in a head end temperature of 260 K corresponding to the steady-state experi-

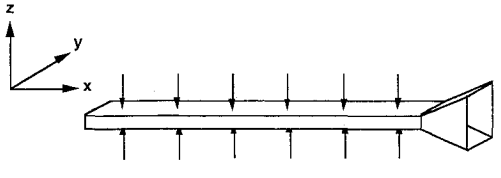

Fig. 1 ONERA cold flow test chamber geometry. Dimensions are $0.48 \times 0.04 \times 0.02$ m, excluding the nozzle.

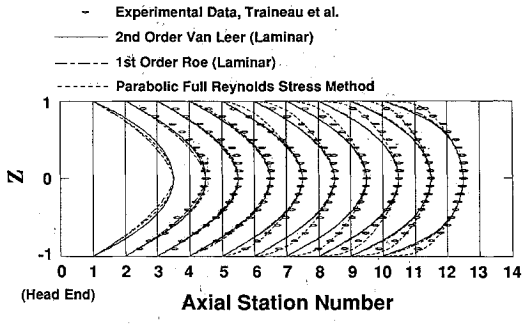

Fig. 2 Comparison of computed normalized axial velocity profiles with ONERA cold flow data.

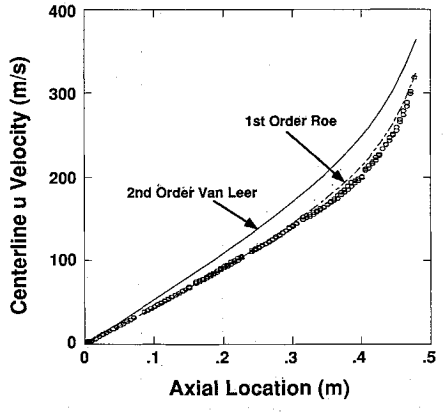

Fig. 3 Computed centerline axial velocity comparison to ONERA cold flow data.

mental result. The approximate injection Reynolds number, $Re_s = 8000$, and the flow character is such that convection terms dominate, even though the flow is turbulent. The CFL number used for this case was approximately 7.5.

Comparisons with the experimental data are given in Figs. 2 and 3. Figure 2 shows normalized axial velocity profiles at the centerplane, where the distance of the axial stations from the head end are 1.1, 5.1, 10.1, 15.1, 20.1, 25.1, 30.1, 35.1, 40.1, and 45.1 cm respectively. The calculations were made using both second-order ($\kappa = -1$) van Leer and first-order ($\phi = 0$) Roe differencing. For additional comparison, results from a parabolic, full Reynolds-stress turbulence model method[23] are also provided. It may be seen that both upwind methods from the current algorithm appear to agree with each other very well except very near the head end. Both of these schemes and the parabolic method agree with the experimental data favorably through the first four stations. The current laminar analysis does not agree with experiment, however, downstream of the fifth axial experimental station at $x/L = 0.42$ since Reynolds stresses become increasingly important. This is verified by the close agreement of the parabolic code with the experimental data at all axial stations.

Although the normalized laminar profiles compare favorably using either scheme, the non-normalized axial centerline velocity shows a very different situation. As seen in Fig. 3, the first-order Roe case agrees with the experimental data extremely well in the laminar portion of the duct. Beyond transition, however, the centerline velocity is overpredicted. This may again be attributed to the laminar assumption of the current model. Second-order van Leer results are found to be in poor agreement on the centerline along the entire length of

Table 3 Pressure comparison to ONERA cold flow experiment

	P_{head} (bar)	P_{exit}/P_{head}
ONERA experiment	3.00	0.417
1st-Order Roe	3.15 (5%)	0.403 (3.4%)
2nd-Order van Leer	3.48 (16%)	0.349 (16%)

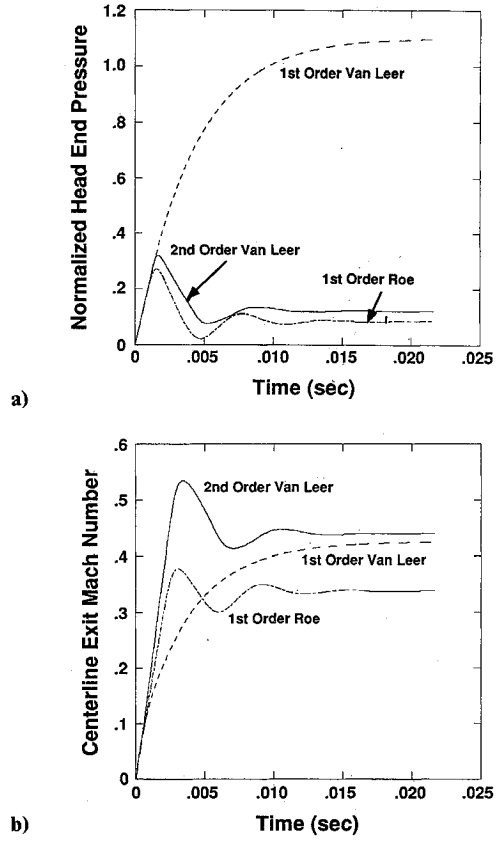

Fig. 4 ONERA subsonic exit test: a) comparison of computed transient pressure; b) comparison of transient exit Mach number.

the duct. These results for an Euler dominated flow present similar findings to those of van Leer et al.[15] for a viscously dominated flow in which it was found that van Leer's flux splitting was overly diffusive.

Comparing further, Table 3 shows the pressure response of the two schemes. Roe's flux splitting is again seen to perform well, with agreement to within 5% of experimental values on a relatively coarse grid.

ONERA Cold Flow Test—Subsonic Exit

The ONERA test chamber geometry of Fig. 1 was used with a decreased injection rate such that the steady, centerline exit Mach number would remain much less than unity. With one characteristic at the exit pointing back upstream, partial reflection of acoustic waves is expected to occur. For this test, the wall injection rate was decreased to $(\rho w)_s = 2.0$ kg/m^2/s (all other conditions remained the same). This case serves to demonstrate the development of simple acoustic waves as a mean flow is established by impulsive injection into a quiescent chamber. The acoustic wave may then be tracked and its speed compared to the theoretical sound speed to determine the time-accuracy of the numerical method.

Figures 4a and 4b illustrate the starting transients. Figure 4a shows the response of the pressure at the head end for three spatial differencing schemes. The large numerical diffusivity of the first-order van Leer scheme is seen to completely absorb any acoustic behavior within one-quarter wavelength. Similar results are seen in the centerline exit Mach number response (Fig. 4b). In both figures, the results from first-order Roe and second-order van Leer are seen to track the acoustic waves and reflect them at the boundaries (an impermeable wall at the head end and open subsonic exit at the aft end).

The numerical data were further analyzed to evaluate the speed of the acoustic wave over a full wavelength (four times the length of the chamber). The characteristic wave speed is $u - a$ for waves traveling upstream and $u + a$ for waves traveling downstream. Mean flow effects were taken into account

Table 4 Comparison of computed and theoretical sound speed

	Sound speed (m/s)	% error
Theory	323	(—)
1st-Order Roe	319	1.2
2nd-Order van Leer	272	15.8

by approximate evaluation of the mean axial velocity in space and time over each quarter wavelength. This was accomplished by assuming a parabolic profile for the velocity along the centerline, and a curve fit of the computed exit velocity as a function of time. This analysis produced the results in Table 4. Roe's method is seen to compare extremely well to acoustic theory with very little error. Van Leer's method, on the other hand, falls well short of an acceptable range of error and was not considered further.

Piston Driven Resonance Tube

Further comparisons have been made to the experimental resonance tube data of Merkli and Thomann.[24] The previous test has demonstrated the ability of the numerical method to compute acoustic waves arising from starting transients in the flow. This test demonstrates the ability of the method to calculate acoustic modes resulting from standing waves and exhibits the ability of the method to establish a resonance condition at a frequency corresponding to that predicted by linear theory. In addition, off-resonance behavior is examined and the wave forms of both cases are compared to experiment. All numerical results are computed using second-order ($\kappa = -1$) Roe flux difference splitting in the axial direction and first-order ($\phi = 0$) Roe radially.

The Merkli and Thomann resonance tube is a simple cylindrical duct 1.7 m long and 9.5 mm in radius. A sinusoidally moving piston is placed at one end with piston amplitude, λ_{max}, variable up to 13.8 mm. The initial ambient conditions are $T = 298$ K and $p = 10^5$ N/m^2 (1 bar). The numerical simulation used an axisymmetric geometry matching the physical dimensions of the tube.

Several comparisons to the Merkli and Thomann data have been made. The first case considered was with a theoretical resonant piston frequency of 102 Hz and piston amplitude, λ_{max}, of 13.8 mm. For resonance to occur, the head and piston end pressure responses are expected to be 180 deg out of phase with each other and have equal amplitudes. Two grids were considered for this case. The first grid used 42 x 50 cells and 96 time steps per cycle. The second grid was higher resolution in space and time, using 63 x 75 cells and 144 time steps per cycle. Fifteen cycles were run on each grid using a Courant number, CFL = 187. The Courant number is defined globally as follows:

$$\mathrm{CFL} \cong a\delta t\left(\frac{1}{\Delta x}+\frac{1}{\Delta y}\right) \tag{24}$$

Figure 5 shows that resonance occurs rapidly and is held throughout the computation. Although resonance was attained similarly on both grids, only the 42 x 50 grid results are shown in Fig. 5. A mean pressure shift is found to occur and corresponds directly to a rise in temperature. This temperature rise may be attributed to the use of an adiabatic wall boundary condition, which causes the irreversible work done by the piston on the fluid (in addition to viscous heating) to be converted directly to a rise in internal (and kinetic) energy of the fluid. Although Fig. 5 shows little evidence, it is expected that a continued temperature rise would result in detuning from resonance. (It is noted that the experimental data was acquired after a 20-min transient period was allowed to elapse.)

Figure 6 compares the computed and experimental wave profiles. The pressure shift of Fig. 5 has been removed from

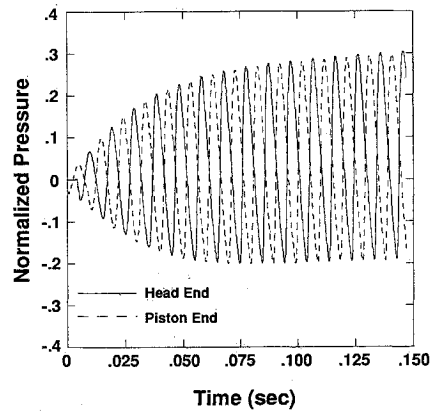

Fig. 5 Resonance tube pressure response for frequency, $f = 102$ Hz, and piston amplitude, $\lambda_{max} = 13.8$ mm (42 x 50 cells, 96 steps/cycle).

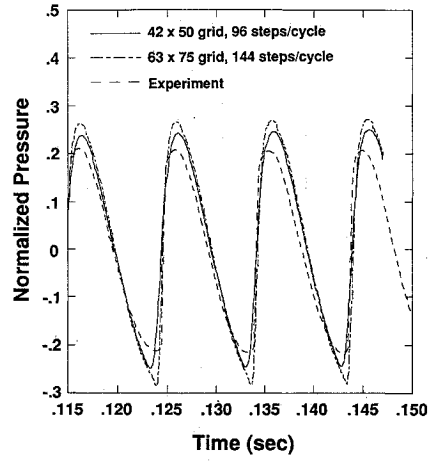

Fig. 6 Comparison of computed and experimental wave profiles at full amplitude resonance, $f = 102$ Hz, $\lambda_{max} = 13.8$ mm.

the computed solutions to facilitate the comparison. Reasonable agreement in amplitudes is seen in all cases (the corresponding Mach number amplitude is 0.17), although the higher resolution calculation results in steeper wave profiles. Most significant, though, is the demonstrated ability to reproduce the N-type traveling wave profile of the experimental resonance condition in each case.

Although a reasonably large Courant number was used for these calculations, it should be noted that the Courant number in the (axial) direction of wave propagation was selected to be unity, i.e.,

$$\mathrm{CFL}_x \cong \frac{a\delta t}{\Delta x} = 1 \tag{25}$$

This is not due to any inherent stability restriction, but rather is intended to limit the introduction of numerical dispersion and dissipation typical of higher CFL numbers for unsteady problems.[25] Through experience it has been observed that this choice of axial CFL number is especially critical for problems in which shocks are expected to occur. When only sinusoidal modes are expected it has been found that a higher axial CFL is possible. This is demonstrated in the off-resonance test to follow.

The ability to attain large radial CFL numbers allows for enhanced spatial resolution of the acoustic boundary layer. Although the current resolution is insufficient for boundary layer analysis, the axial velocity near the pressure node does show the classical Richardson maximum in axial velocity.[26] The results of higher-resolution acoustic boundary-layer analysis will be presented in a future paper.

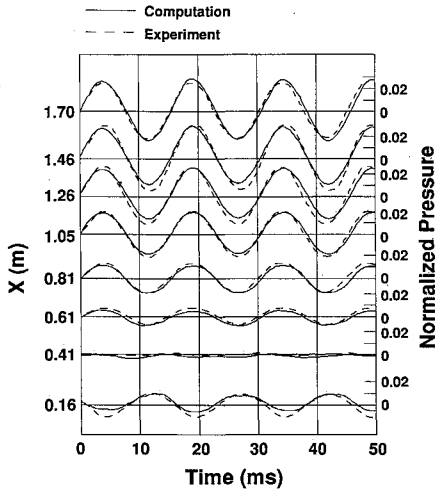

Fig. 7 Comparison of computed and experimental off resonance results, $f = 65.3$ Hz, $\lambda_{max} = 13.8$ mm.

A final test was conducted with the resonance tube by comparing with experimental off-resonance data, which are well characterized by classical linear-acoustic standing-wave motions. The driving frequency in this case was 65.3 Hz with a piston amplitude of 13.8 mm. This case was computed on a 42×50 grid using a CFL number of 590, corresponding to 48 time steps per cycle. In this case the axial Courant number was 2.72. This was considered reasonable since no shocks occur and yields acceptable truncation error in computed mode shapes. Further tests have revealed that a very high axial Courant number (obtained by reducing axial spacing by an order of magnitude) gives nearly identical results to those shown here. Figure 7 shows a comparison of the computed results with the experimental results at these conditions. Again, good agreement is seen. The pressure amplitudes at all axial locations compare very well, as does the computed location of the pressure node.

Timing of the off-resonance case was also used for comparison of efficiency with other methods. The current method was timed on a Cray X-MP/48 (using a single processor) to require 25.7 ms/grid cell/cycle. Vuillot and Avalon[5] used a Cray X-MP/18 and required 450 msec/grid cel/cycle (using 3571 steps per cycle). Though no specific timing information was given by Baum and Levine,[9] the code used was the same as that of Sabnis et al.[27] (including a two-equation turbulence model). From the information provided by Ref. 27 it was inferred that approximately 40 ms/grid cell/cycle were required in Ref. 9 (using 300 steps per cycle).

IV. Conclusions

An implicit, time-accurate, iterative upwind method has been developed and applied to three test cases. Although several researchers have discarded implicit methods for time-accurate solutions, the results from these tests clearly show a strong potential for implicit methods when properly formulated. The current method has demonstrated accurate propagation of acoustic information and good convergence characteristics for steady-state problems. The computational efficiency lost by the incomplete vectorization of iterative methods is overcome by operating at relatively large CFL numbers, $O(10^2)$. The CFL numbers used for this work were found not to be limited by stability restrictions. It was found, however, that the CFL number in the direction of wave propagation should be limited to order unity to avoid excessive dispersive and dissipative errors for nonlinear motions.

The test cases considered have yielded encouraging results. In particular, it is felt that the resonance tube problem provides a challenging physical situation for comparison. In addition to its simple configuration, comparisons with detailed data have provided a critical test for validating time-accuracy.

Acknowledgments

This research was supported, in part, by the Société Nationale des Poudres et Explosifs, Centre des Recherches du Bouchet. The first author also wishes to acknowledge the support of NASA Marshall Space Flight Center under fellowship Grant NGT-50363. Supercomputing time on the Cray X-MP/48 and Cray 2 computers was provided by the National Science Foundation and the National Center for Supercomputing Applications.

References

[1]Williams, F. A., *Combustion Theory,* 2nd ed., Benjamin/Cummings, Menlo Park, CA, 1985, Chap. 9.

[2]Strehlow, R. A., *Combustion Fundamentals,* McGraw-Hill, New York, 1984, Chap. 14.

[3]Kailasanath, K., Gardner, J. H., Boris, J. P., and Oran, E. S., "Acoustic-Vortex Interactions and Low-Frequency Oscillations in Axisymmetric Combustors," *Journal of Propulsion and Power,* Vol. 5, No. 2, 1989, pp. 165–171.

[4]Yang, V., Hsieh, K. C., and Tseng, I. S., "Velocity-Coupled Flow Oscillations in a Simulated Solid-Propellant Rocket Environment," AIAA Paper 88-0543, Jan. 1988.

[5]Vuillot, F., and Avalon, G., "Acoustic-Mean Flow Interaction in Solid Rocket Motors Using Navier-Stokes Equations," AIAA Paper 88-2940, July 1988.

[6]Lindemuth, I., and Killeen, J., "Alternating Direction Implicit Techniques for Two-Dimensional Magnetohydrodynamic Calculations," *Journal of Computational Physics,* Vol. 13, Oct. 1973, pp. 181–208.

[7]Beam, R. M., and Warming, R. F., "An Implicit Factored Scheme for the Compressible Navier-Stokes Equations," *AIAA Journal,* Vol. 16, No. 4, 1978, pp. 393–402.

[8]Briley, W. R., and McDonald, H., "Solution of the Three-Dimensional Compressible Navier-Stokes Equations by an Implicit Technique," *Proceedings of the Fourth International Conference on Numerical Methods in Fluid Dynamics, Lecture Notes in Physics,* Vol. 35, Springer-Verlag, New York, 1975, pp. 105–110.

[9]Baum, J. D., and Levine, J. N., "Numerical Investigation of Acoustic Refraction," *AIAA Journal,* Vol. 25, No. 12, 1987, pp. 1577–1586.

[10]Tang, W., Sankar, L. N., and Strahle, W. C., "Numerical Simulation of Vorticity Acoustics Interactions within Dump Combustors," AIAA Paper 88-0597, Jan. 1988.

[11]Chakravarthy, S. R., "Relaxation Methods for Unfactored Implicit Upwind Schemes," AIAA Paper 84-0165, Jan. 1984.

[12]Steger, J. L., and Warming, R. F., "Flux Vector Splitting of the Inviscid Gasdynamic Equations with Application to Finite-Difference Methods," *Journal of Computational Physics,* Vol. 40, April 1981, pp. 263–293.

[13]Van Leer, B., "Flux-Vector Splitting for the Euler Equations," *Lecture Notes in Physics,* Vol. 170, 1982, pp. 507–512.

[14]Roe, P. L., "Approximate Riemann Solvers, Parameter Vectors, and Difference Schemes," *Journal of Computational Physics,* Vol. 43, Oct. 1981, pp. 357–372.

[15]Van Leer, B., Thomas, J. L., Roe, P. L., and Newsome, R. W., "A Comparison of Numerical Flux Formulas for the Euler and Navier-Stokes Equations," AIAA Paper 87-1104, June 1987.

[16]Thomas, J. L., and Walters, R. W., "Upwind Relaxation Algorithms for the Navier-Stokes Equations," *AIAA Journal,* Vol. 25, No. 4, 1987, pp. 527–534.

[17]Peyret, R., and Viviand, H., "Computation of Viscous Compressible Flows Based on the Navier-Stokes Equations," *AGARDograph* 212, 1975.

[18]Warming, R. F., and Beam, R. M., "On the Construction of Implicit Factored Schemes for Conservation Laws," *SIAM-AMS Proceedings,* Vol. 11, 1978, pp. 85–129.

[19]Hanel, D., Schwane, R., and Seider, G., "On the Accuracy of Upwind Schemes for the Solution of the Navier-Stokes Equations," AIAA Paper 87-1105, June 1987.

[20]Van Leer, B., "Towards the Ultimate Conservative Difference Scheme. V. A Second-Order Sequel to Godunov's Method," *Journal of Computational Physics,* Vol. 32, July 1979, pp. 101–136.

[21]Godunov, S. K., "A Difference Method for the Numerical Calcu-

lation of Discontinuous Solutions of Hydrodynamic Equations," *Matematiceskii Sbornik,* Vol. 47, 1959, pp. 271–306.

[22]Traineau, J-C., Hervat, P., and Kuentzmann, P., "Cold-Flow Simulation of a Two-Dimensional Nozzleless Solid Rocket Motor," AIAA Paper 86-1447, 1986; also Hervat, P., "Simulation De L'Ecoulement Des Produits De Combustion Dans Un Propulseur A Propergol Solide Sans Tuyere," Ph.D. Dissertation, CNAM, Paris, June 1986.

[23]Beddini, R. A., "Injection Induced Flows in Porous Walled Ducts," *AIAA Journal,* Vol. 24, No. 11, 1986, pp. 1766–1773.

[24]Merkli, P., and Thomann, H., "Thermoacoustic Effects in a Resonance Tube," *Journal of Fluid Mechanics,* Vol. 70, July 1975, pp. 161–177.

[25]Hsieh, K.-C., "Assessment of Numerical Techniques for Unsteady Flow Calculations," AIAA Paper 89-1956, June 1989.

[26]Schlichting, H., *Boundary Layer Theory,* 7th ed., McGraw-Hill, New York, 1979, Chap. 15.

[27]Sabnis, J. S., Gibeling, H. J., and McDonald, H., "Navier-Stokes Analysis of Solid Propellant Rocket Motor Internal Flows," *Journal of Propulsion and Power,* Vol. 5, No. 6, 1989, pp. 657–664.